Influence of EMAA Compatibilizer on the Structure and Properties of HDPE/Hydrotalcite Nanocomposites Prepared by Melt Mixing

M. Ardanuy,[1] J. I. Velasco,[1] M. L. Maspoch,[1] L. Haurie,[2] A. I. Fernández[3]

[1]*Centre Català del Plàstic, Universitat Politècnica de Catalunya, C/Colom 114, E-08222 Terrassa, Spain*
[2]*Escola Politècnica Superior d'Edificació de Barcelona, Laboratori de Materials, Universitat Politècnica de Catalunya, Avinguda Dr. Marañón, 44-50, E-08028 Barcelona, Spain*
[3]*Departament de Ciència dels Materials i Enginyeria Metallúrgica, Universitat de Barcelona, Martí i Franquès 1, E-08028 Barcelona, Spain*

Received 16 September 2008; accepted 23 January 2009
DOI 10.1002/app.30133
Published online 30 March 2009 in Wiley InterScience (www.interscience.wiley.com).

ABSTRACT: High-density polyethylene (HDPE)/hydrotalcite nanocomposites were prepared and characterized with a partially neutralized sodium ionomer of poly(ethylene-*co*-methacrylic acid) (EMAA) as a compatibilizer. Moreover, nanocomposites based on this ionomer were characterized as patterns to analyze the interactions between the hydrotalcite sheets and the methacrylic groups on the ionomer. Hydrotalcite particles were organically modified with sodium dodecyl sulfate ions. Their presence in the interlayer space was confirmed by means of Fourier transform infrared spectroscopy (FTIR) and X-ray diffraction (XRD). Morphological analysis carried out with XRD and transmission electron microscopy (TEM) revealed the partially exfoliated/intercalated structure achieved in the nanocomposites. The mechanical properties of the HDPE nanocomposites mainly depended on the nature of the polymer matrix. Higher values of the tensile strength and Young's modulus were found in the EMAA nanocomposites. Thermogravimetric analysis (TGA) showed that hydrotalcite particles improved the thermal stability and delayed the onset decomposition temperature of both HDPE and EMAA nanocomposites. © 2009 Wiley Periodicals, Inc. J Appl Polym Sci 113: 950–958, 2009

Key words: clay; ionomers; nanocomposites; polyethylene (PE); thermogravimetric analysis (TGA)

INTRODUCTION

Synthetic anionic clays, such as hydrotalcite (HT)-type materials, have received considerable attention in recent years.[1–5] The use of HT as a nanofiller represents an emerging field of application, and HT may offer advantages in comparison with montmorillonite because of the versatility of its chemical compositions and its modifiable charge density, which allow multiple interactions with polymers. Besides, HT contains a large number of hydroxide groups in its structure, and this makes it interesting as a fire-retardant additive for polymers.

HT compounds are layered double hydroxides (LDHs) with magnesium–aluminum (Mg–Al) hydroxide based layers and carbonate ions in the interlamellar space. They are represented by the general formula $[Mg_{1-x}Al_x(OH)_2](CO_3)_{x/2}{\cdot}mH_2O$, where $0.25 < x < 0.33$.[6] HT is the most common LDH used to prepare hybrid organic–inorganic layered materials and can be produced in a very pure form. The platelets are positively charged, in contrast to the negative charge found in montmorillonite, so its interlayer space is occupied by anions. The HT structure allows the exchange of the interlamellar inorganic anions with organic ones.[7] LDH sheets are composed of one polyhedra-made layer, which is often corrugated, and are therefore more flexible than other two-dimensional frameworks such as 2 : 1 layered silicate.

Because of the lack of polar groups in the polyethylene (PE) backbone, it is difficult to obtain an exfoliated and homogeneous dispersion of the clay platelets at a nanometer level. Therefore, the modification of the matrix with polar groups becomes necessary. PE modified with maleic anhydride as a compatibilizer has proven to be favorable for the exfoliation of montmorillonite[8,9] and HT particles.[10,11] Other less studied approaches to improving PE/clay compatibility include the use of copolymers of ethylene with acrylic acid or methacrylic acid (MAA). In this sense, different studies have proven the effectiveness of poly(ethylene-*co*-methacrylic acid) (EMAA)

Correspondence to: M. Ardanuy (monica.ardanuy@upc.edu).

ionomers with cationic clays.[12–14] This effectiveness has been attributed to the interactions of the ionic and acid groups in these ionomers with the aluminosilicate surface of the clay.

Ionomers are polymers with a small molar fraction of ionic groups covalently bonded to the polymer backbone. A well-known commercial ionomer is a copolymer of ethylene and MAA, which is marketed under the name Surlyn. It is expected that the ionic groups on the ionomer (negatively charged) will have favorable interactions with the HT platelets (positively charged).

Different studies have reported the preparation and characterization of nanocomposites based on PE and LDHs. Nevertheless, these works have focused on low-density polyethylene (LDPE)[15,16] or linear low-density polyethylene,[17] and high-density polyethylene (HDPE)/LDH nanocomposites are scarcely described in the literature. *In situ* polymerization and solution intercalation are the most common methods used to prepare polymer/LDH nanocomposites. Nevertheless, for large-scale industrial applications, the melt-mixing process is a more environmentally friendly and convenient process because of the absence of organic solvents. Moreover, this method is compatible with current industrial processes such as extrusion and injection molding.

Most PE consumption is for packaging applications. Its very good balance of optical and mechanical properties makes it ideal for food and pharmaceutical packaging applications. However, although PE has acceptable moisture barrier characteristics, it has poor barrier characteristics with respect to oxygen and carbon dioxide. The incorporation of a small quantity of HT into PE is expected to enhance the mechanical, barrier, and thermal properties simultaneously. Improvements in both the mechanical and barrier properties of the films will benefit current applications and lead to more advanced applications.

In this work, we describe the preparation, structural characterization, and thermal and mechanical properties of nanocomposites based on HT and HDPE. With the aim of obtaining a system with well-dispersed HT particles and a good affinity between the filler and the polymer, the carbonate anions in the inner gallery space of the HT were exchanged with dodecyl sulfate ones. We expected a decrease in the interactions between the layers to allow polymer chain intercalation and exfoliation of the HT layers. EMAA ionomer, partially neutralized with sodium ions, was used to improve the interactions between the nonpolar backbone of the PE and the inorganic particles. As far as we know, the use of an ionomeric compound as a compatibilizer in PE/HT nanocomposites has not been reported in the literature. In addition, nanocomposites were also made from this ionomer so that we could better understand the interactions between their ionic groups and the HT particles.

EXPERIMENTAL

Materials

HDPE [density = 0.950 g/cm^3, melt flow index (MFI) = 1 g/10 min] was supplied by Repsol YPF (Tarragona, Spain). EMAA ionomer (Surlyn 8920) was purchased from DuPont (Barcelona, Spain). This ionomer is an ethylene and MAA copolymer in which some of the acid groups (5.4 mol %) have been partially neutralized to form the sodium salt (60% of the acid groups).

Synthetic HT (Hycite 713), supplied by Ciba (Barcelona, Spain), was used as the Mg–Al LDH precursor. Sodium dodecyl sulfate was purchased from Aldrich Chemical Co. (Madrid, Spain).

Organic modification of HT

Organophilized HT [hydrotalcite dodecyl sulfate (HTDS)] was prepared in two steps that combined the reconstruction and ion-exchange methods.[6,7] First, NaCl salt and calcined HT were mixed in an aqueous solution and stirred to form HT with chloride anions (HTCl). In a second step, the HTCl paste was stirred in an aqueous sodium dodecyl sulfate solution at 80°C for 3 days. The dodecyl sulfate concentration was twice the theoretical amount of the ion-exchange capacity of HTCl. A white precipitate (HTDS) was separated by filtration, washed with deionized water, and dried *in vacuo* at 65°C for 24 h.

Preparation of the nanocomposites

Nanocomposites containing pure or organically modified HT (10 wt %) were prepared on a Collin ZK-35 corotating twin-screw extruder (diameter = 25 mm, length/diameter = 36). The screw speed was fixed at 60 rpm, and the melting temperature of the mass at the die was 160°C. Table I summarizes the compositions of the prepared nanocomposites.

Discs (3 mm thick) and square plaques (1 mm thick) were compression-molded with a hot-plate press. Different specimens were machined to characterize the prepared materials.

Measurements

Fourier transform infrared (FTIR) spectra were recorded in the wave-number range of 400–4000 cm^{-1} with a Nicolet 510 FTIR spectrometer.

TABLE I
Nominal Compositions and Crystallization and Melting Characteristics Obtained from DSC

Sample	Composition (wt %)	MFI (g/10 min)	Density (g/cm^3)	T_m (°C)	T_c (°C)	X_m (%)	X_c (%)
PE	HDPE	1.03	0.953	130.0	116.4	85.0	84.4
PEHT	HDPE/HT (90/10)	1.01	1.001	130.7	116.7	85.4	83.0
PEHTDS	HDPE/HTDS (90/10)	0.75	0.983	130.6	116.6	83.7	84.3
PES	HDPE/EMAA	1.36	0.952	130.7	116.7	85.4	83.0
PESHT	HDPE/EMAA/HT (88/2/10)	0.84	1.001	131.3	116.4	81.7	84.5
PESHTDS	HDPE/EMMA/HTDS (88/2/10)	0.72	0.980	131.5	116.1	82.6	83.5
				T_{m1} (°C)	T_{m2} (°C)	ΔH_{m1} (°C)	ΔH_{m2} (°C)
S	EMAA	0.94	0.953	51.3	88.5	13.9	43.4
SHT	EMAA/HT (90/10)	0.08	0.990	54.7	87.4	15.5	43.8
SHTDS	EMAA/HTDS (90/10)	0.07	0.974	56.0	86.3	15.3	43.4

ΔH_{m1} = first melting enthalpy; ΔH_{m2} = second melting enthalpy; T_c = crystallization peak temperature; T_m = melting peak temperature; T_{m1} = first melting peak temperature; T_{m2} = second melting peak temperature; X_c = crystallinity from crystallization signals; X_m = crystallinity from melting signals.

Samples were prepared through the mixing of 3 wt % HT powders with optical-spectrum-grade KBr.

X-ray diffraction (XRD) analysis was performed in a Siemens D-500 diffractometer using Cu Kα radiation (wavelength = 0.154 nm) and operated at 40 kV and 30 mA. Data were collected in the angular range of 2–60° with 0.02°/min (2θ) scan increments. The interlayer distance of the HT particles was calculated from the (003) diffraction signal with the Bragg equation.

Information about the morphology and distribution of the HT particles was obtained with transmission electron microscopy (TEM). Microtomed sheets 200 nm thick were observed on a JEOL 1200-EXII microscope.

MFI was measured with a melt flow indexer (190°C and 2.16 kg).

Differential scanning calorimetry (DSC) measurements were performed with a PerkinElmer Pyris 7 calorimeter. Calibration of the instrument was done with standard samples of indium and lead. Once the sample thermal history was erased (3 min at 180°C), a cooling cycle was conducted from 180 to 25°C, and after it, a heating run between 25 and 180°C was performed. All runs were carried out at 10°C/min in a stream of dried nitrogen. Samples of 10 mg were used in each case.

The degree of crystallinity (X_m) of HDPE was calculated with the following equation:

$$X_m = \frac{\Delta H_m (m_c/m_p)}{\Delta H_0} \times 100 \quad (1)$$

where ΔH_m is the melting enthalpy experimentally calculated from DSC analysis, ΔH_0 is the theoretical enthalpy of 100% crystalline HDPE (ΔH_0 = 293 J/g[18]), m_c is the mass of the sample, and m_p is the mass of HDPE in the sample.

Thermogravimetric analysis (TGA) was carried out in an air atmosphere with a Setaram TG-DTA 92. The heating rate was 5°C/min.

The limiting oxygen index (LOI) and UL94 vertical burning test were used to characterize the flame behavior of the prepared nanocomposites. The LOI measurements were carried out according to UNE-EN ISO 4589-2 with 120 × 10 × 1 mm^3 specimens. The UL94V testing was carried out with 127 × 12 × 1 mm^3 specimens.

Tensile tests were carried out with a Galdabini Sun 2500 dynamometer according to ASTM Standard D 638. The experiments were conducted at room temperature with a deformation rate of 10 mm/min. From the obtained tensile curves, average values of tensile strength, neck propagation strength, and Young's modulus were determined. At least five specimens were tested for each composition.

RESULTS AND DISCUSSION

Structural characterization of pure HT and organically modified HT

The FTIR spectra of pure HT and organically modified HT (HTDS) are shown in Figure 1. The spectrum of HT has a broad absorption band around 3470 cm^{-1}. This band occurs as the result of overlapping of the stretching mode of the hydroxyls attached to Al and Mg and the shoulder due to hydrogen bonding of the interlayer water and interlayer carbonate. At 1650 cm^{-1}, the bending mode of interlayer water can be observed. At 1372 cm^{-1}, the band assigned to the antisymmetric υ_3 mode of interlayer carbonate ions appears. In the 1200–400 cm^{-1} region, different absorption bands appear that are attributable to the Al—O stretching modes (960, 780, and 560 cm^{-1}) and M—O stretching mode (680 cm^{-1}). These bands appear overlapped with other bands that are attributed to the υ_2 mode (at 865 cm^{-1}) and the υ_4 mode (at 660 cm^{-1}) of carbonate ions. The spectrum of HTDS shows new absorption bands at 2921 and 2852 cm^{-1}, which are attributable to the C—H stretching vibration of the

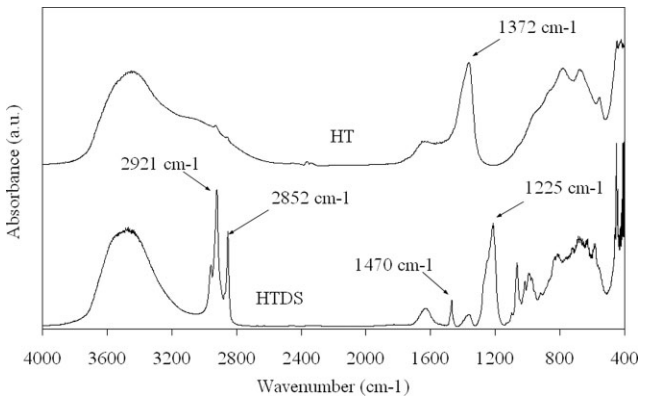

Figure 1 FTIR spectra of pure HT and organophilized HT.

aliphatic chain of sodium dodecyl sulfate ion, and at 1470 and 1220 cm^{-1}, which are attributable to the S=O stretching vibration of the sulfate group. The presence of these new bands and the considerable decrease in the intensity of the characteristic band of the carbonate stretching mode (1372 cm^{-1}) indicate the exchange of the carbonate ions in the interlayer space of the HT by dodecyl sulfate ones.

The XRD spectra of HT and HTDS are shown in Figure 2. The diffraction planes have been indexed on the basis of a hexagonal unit cell. As shown in this figure, dodecyl sulfate insertion into the HT gallery resulted in a shift of the (003) diffraction plane from $2\theta = 11.48$ for HT to $2\theta = 3.33$ for HTDS. This shifting caused an increase in the d spacing (d_{003}), which was calculated with the Bragg equation and passed from 0.77 nm for pure HT to 2.65 nm for the organically modified HT. d_{003}, usually called the interlayer spacing, includes a contribution from the metal hydroxide sheet (ca. 4.8 Å) and the gallery region that contains the intercalated anions. As shown, the incorporation of the dodecyl sulfate anions resulted in a significant increase in the gallery height. Under the assumption that the HT sheet structure was not affected by the incorporation of dodecyl sulfate, this expansion of HT along the c axis caused the unit cell volume to expand. This larger space between the Mg–Al layers promoted the intercalation of the polymer, leading to easy exfoliation of the HT sheets in the polymer matrix.

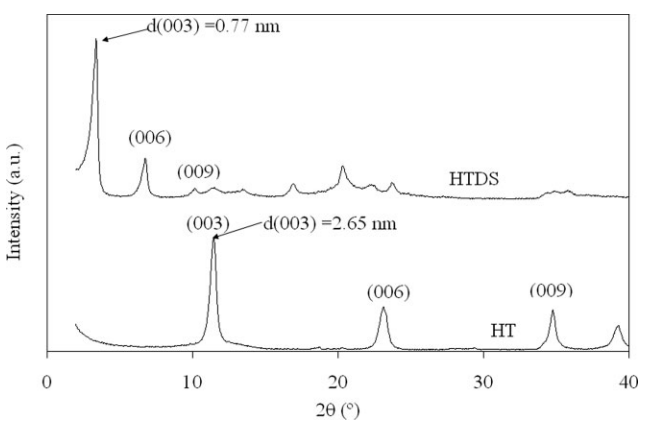

Figure 2 XRD patterns of pure HT and organophilized HT.

Structural characterization of the HDPE and EMAA nanocomposites

The XRD patterns of the HDPE/HT nanocomposites are shown in Figure 3. When the nanocomposites were prepared with pure HT, no significant change in the position of the basal peak (003) of the HT particles resulted for the PEHT and PESHT samples, and this indicated that an important fraction of HT particles maintained their original structure in the PE matrix. Nevertheless, a substantial reduction of the intensity of this peak occurred in PESHT with respect to PEHT. Because the content of HT particles was similar in the two samples, this reduction suggested an eventual partial exfoliation of these particles in the PES matrix, which was probably favored by the presence of the ionomer.

When HTDS was used, as shown in Figure 3, the (003) plane diffraction peak of the clay was shifted to lower angles in the nanocomposites, and so the interlayer spacing of HTDS increased from 2.6 to 3.2 and 4.2 nm in the PESHTDS and PEHTDS samples, respectively. This increase could be due to the intercalation of polymer chains in the interlamellar space of the HT. Furthermore, all the diffraction peaks of HTDS became broader and of lower intensity in the nanocomposites. Therefore, a disordering of the HTDS crystals was apparent, showing how these particles were partially exfoliated and intercalated in both the PE and PES matrices.

A general decrease of the MFI was observed in the nanocomposites (Table I). Moreover, differences, depending on the composition that supported the

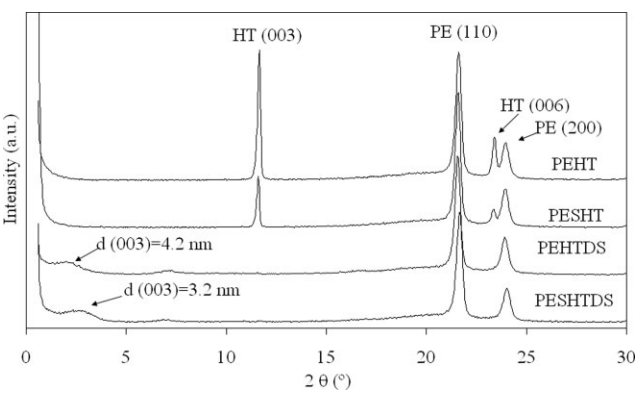

Figure 3 XRD patterns of HDPE/HT nanocomposites.

structures elucidated by XRD, should be noted. On the one hand, lower MFI values resulted in nanocomposites prepared with HTDS, and on the other hand, in the nanocomposites prepared with HT particles, a significantly lower MFI value resulted for PESHT with respect to PEHT. Increased viscosities at lower shear forces are observed in nanocomposites with a certain exfoliation grade as a result of the higher surface contact between the layers and polymer matrix. In the prepared nanocomposites, the differences observed in the viscosity values could be related to different grades of exfoliation of the HT particles achieved in the HDPE or HDPE/EMAA matrix. HT particles were only partially exfoliated in the HDPE/EMMA matrix, and as a result, a lower value of MFI was obtained in the PESHT sample. HTDS particles were exfoliated to a similar extent in both the HDPE and HDPE/EMAA matrices, and as expected, similar MFI values resulted for the PEHTDS and PESHTDS nanocomposites.

TEM revealed the very complex nature of the morphology of the dispersed HT particles, which varied widely in size and shape. The presence of exfoliated particles in the PEHTDS and PESHTDS samples can be observed in the high-magnification TEM images illustrated in Figure 4(a), which corroborates the XRD results.

Two broad signals that appeared at 4.2 and 20.7° could be observed in the spectrum of pure EMAA (Fig. 5). The first signal is usually related to the formation of ionic aggregates (known as the ionic signal), and the second one is related to the superpositioning of the signals of the (110) and (200) diffraction planes of the crystalline phase of PE. As shown in this figure, the two original peaks of HT remained in the SHT sample. Nevertheless, a substantial reduction of the intensity of the peaks must be noted, indicating an eventual partial exfoliation of the HT particles. When HTDS particles were

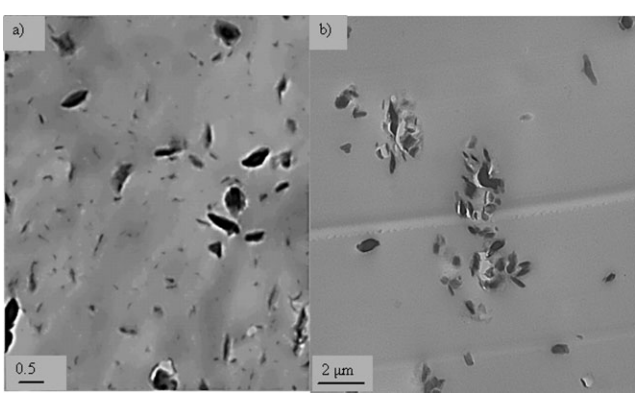

Figure 4 TEM images of (a) the general morphology shown by HDPE/EMAA/HTDS nanocomposites and (b) the agglomeration of HTDS particles into the EMAA matrix.

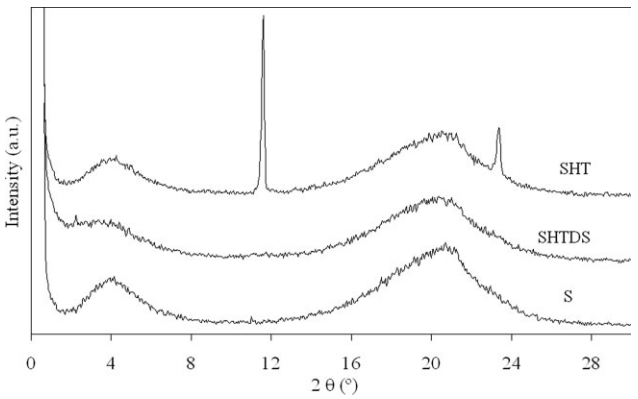

Figure 5 XRD patterns of EMAA/HT nanocomposites.

used, the (003) diffraction peak disappeared in the SHTDS pattern, and this indicated that almost complete exfoliation of the LDH layers was achieved.

The largest agglomerates of HT particles, probably caused by strong ionic interactions between the MAA groups of the ionomer and the cationic layers of HT, were observed in TEM images of EMAA nanocomposites [Fig. 4(b)].

MFI of the resultant EMAA was strongly modified by the effects of both HT and HTDS particles, and this confirmed the existence of very high ionic interaction forces between the HT sheets and the MAA groups, which significantly reduced the flow of the ionomer. Vanhoorne and Register[19] theorized that in the melt state, ionomers flow because of a mechanism known as ion hopping. The diffusion (hopping) of ionic groups among aggregates permits relaxation of stresses within the segment of the polymer chain attached to the ionic group. Because of this relaxation mechanism, macromolecules can diffuse without involving the simultaneous ion hopping of all the ionic associations along the chain, and the likelihood of these occurring decreases with increasing ionic character. Because the ionic associations act as physical (temporary) crosslinks, there is a net decrease in the diffusion coefficient of the chains resulting in an increase in viscosity. In this sense, the substitution of sodium ions by the cationic sheets of HT, which are less labile, would hinder the flow of the ions between aggregates, resulting in an increase of the viscosity.

Thermal results from DSC (Table I) showed that the melting and crystallization peak temperatures as well as the degree of crystallinity of HDPE were practically unaffected by both pure HT and organically modified HT, and this indicated that these particles did not act as nucleating agents and did not have any influence on the crystallinity degree (at the rate measured) of HDPE. Nevertheless, interesting changes could be observed in the thermal transitions of EMAA when these layered particles were

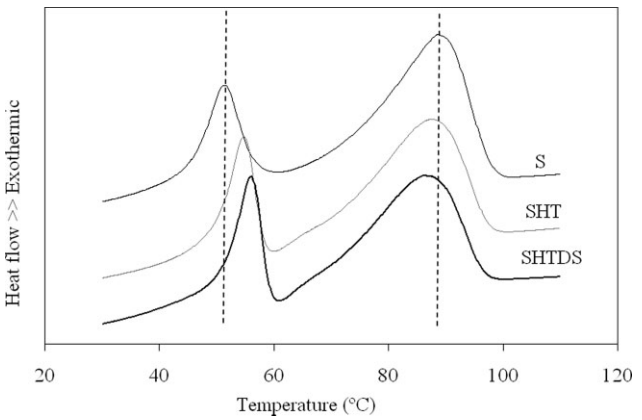

Figure 6 DSC melt thermograms for pure EMAA and EMAA nanocomposites at the cooling rate of 10°C/min.

incorporated. In the first heating of EMAA and EMAA nanocomposites (Fig. 6), two transitions could be observed. The first one (ca. 50°C) is known as the order–disorder transition of the ionic clusters, and the second one (ca. 90°C) is related to the melt process of PE crystals.[20,21] As shown in this figure, the order–disorder transition was shifted from 51.3°C for pure EMAA to 54.7 and 56.0°C for SHT and SHTDS, respectively (Table I). If we assume that this transition could be related to a disarrangement of the ionic aggregates, this increase in the order–disorder transition temperature supports the formation of more stable ionic aggregates when HT particles are in the matrix, especially with the organically modified ones. With respect to the second transition, a slight decrease in the temperature peak resulted in nanocomposites, and this indicates that HT particles probably introduce a certain degree of disorder into the PE matrix.

Thermal stability

TGA plots of HDPE nanocomposites are shown in Figure 7. The thermal decomposition of pure HDPE occurs in one step in the temperature region between 350 and 475°C. Usually, the comparison of the thermal stability of polymeric materials from TGA plots is carried out in terms of two temperatures: the onset-of-decomposition temperature at which 10% weight loss takes place and the decomposition temperature at which 50% weight loss takes place ($T_{50\%}$). The onset of the decomposition of HDPE was significantly delayed by the effect of the organophilized HT particles (from 373°C in HDPE to 386 and 388°C in PEHTDS and PESHTDS, respectively). Nevertheless, pure HT caused only a slight delay (from 373°C in HDPE to 376°C in PEHT). Similarly, $T_{50\%}$ of HDPE increased with the effect of HTDS particles, and this increase was more noticeable in the nanocomposite prepared with the ionomer. The exfoliated platelets probably hindered the diffusion of the gases to a higher degree in agreement with the higher values of the residue obtained for the nanocomposites prepared with the organophilized HT. Additionally, the endothermic decomposition of the host metal hydroxide layer provided a cooling effect that could delay the combustion process of the organic species (surfactant anion, polymer chain segments, etc.) constrained within the gallery space of the HT particles. Similar results were observed by Costa et al.[22] in LDPE/HT nanocomposites.

The thermal decomposition of EMAA is also characterized by one step of weight loss with the maximum around 434°C (Fig. 8). As shown, the thermal stability of this ionomer was strongly improved by the presence of HT particles, which increased the onset temperature from 386 to 410°C and $T_{50\%}$ from 432 to 448°C. Similarly to HDPE nanocomposites, the HT particles hindered the diffusion of the gases.

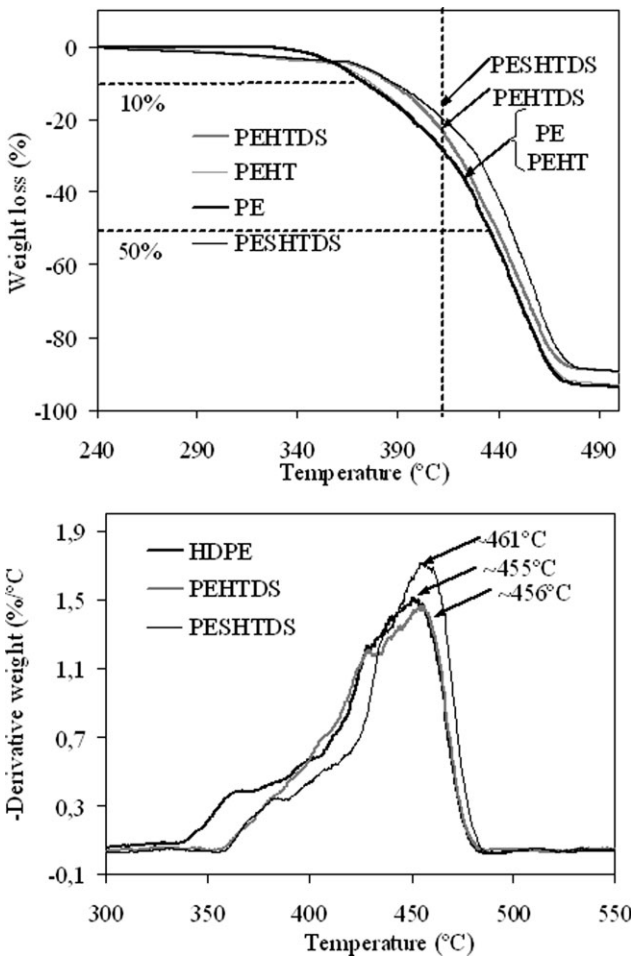

Figure 7 TGA plots of HDPE/HT nanocomposites.

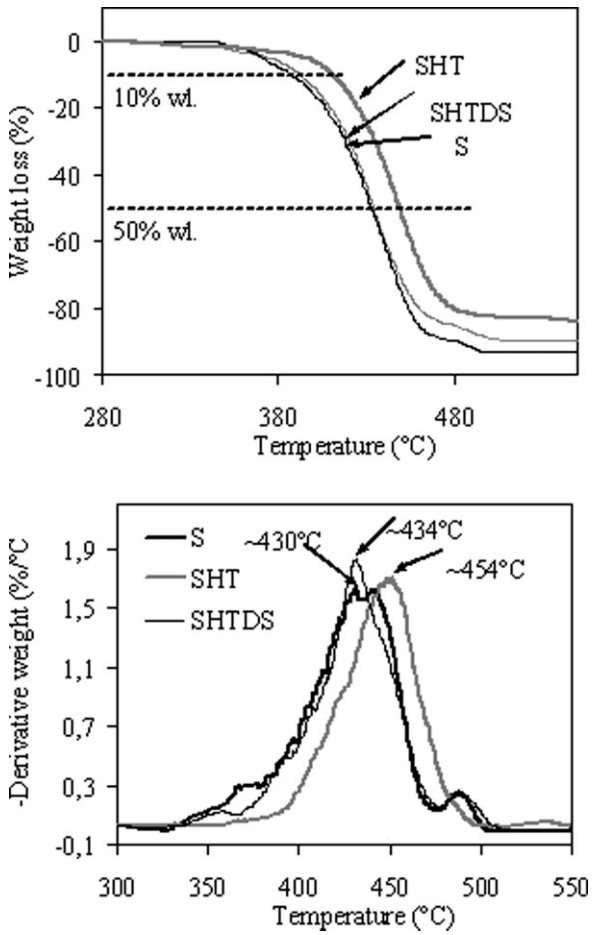

Figure 8 TGA plots of EMAA/HT nanocomposites.

Flame behavior

UL94V testing gives useful information regarding the dripping behavior of nanocomposites. Dripping of burning melts can increase the spread of flames in a real fire. Although all the samples showed dripping while burning, the time at which dripping started was significantly increased by the presence of pure and organophilized HT particles (Table II). For HDPE nanocomposites, this increase was more significant in the samples prepared with the organophilized HT. The highest value was obtained in the PEHTDS nanocomposite. This delayed dripping tendency could be related to the higher melt viscosity of the nanocomposite composition. As can be seen, the higher the viscosity was of the HDPE/HT nanocomposite, the higher its resistance was against dripping during burning.

In EMAA nanocomposites, the highest dripping time was found for the SHT nanocomposite.

The LOI values of HDPE and EMAA did not improve with the addition of the HT particles, being very similar in the nanocomposites with respect to the pure polymers. Only a slight increase was achieved in the PEHTDS nanocomposite (from 18.4% for HDPE to 19.2% for PEHTDS). These values are in agreement with the ones obtained for LDPE/HT nanocomposites by Costa et al.[22] These authors explained this behavior by inefficient char formation in these nanocomposites, indicating that a much higher filler loading would be required in these nanocomposites to obtain LOI values similar to those of conventional polyolefin/metal hydroxide flame-retardant composites.

Mechanical properties

The main characteristics of the mechanical properties, characterized by means of standard tensile testing, are listed in Table II, and the comparative tensile behavior is shown in Figures 9 and 10. Young's modulus of HDPE is almost the same as that of the nanocomposites, independent of the treatment of the particles and the presence of a compatibilizer. This behavior can be explained by the high values of the crystallinity degree calculated by DSC,

TABLE II
Tensile Properties at 10 mm/min and Flammability Results for HDPE/HT and HDPE/EMAA/HT Nanocomposites

Sample	Young's modulus (MPa)	Tensile strength (MPa)	Neck propagation strength (MPa)	Time to start dripping (s)[a]	LOI (% O_2)
PE	1207 ± 101	19.7 ± 0.7	11.4 ± 0.5	12	18.4
PES	1180 ± 201	19.7 ± 1.0	12.1 ± 1.3	13	18.5
PEHT	1433 ± 210	18.7 ± 0.7	11.0 ± 0.8	19	18.7
PESHT	1352 ± 174	20.1 ± 0.4	11.6 ± 0.6	15	18.5
PEHTDS	1185 ± 143	19.6 ± 0.3	11.6 ± 0.4	26	19.2
PESHTDS	1270 ± 89	20.1 ± 0.9	12.4 ± 0.1	20	18.3
S	350 ± 49	16.7 ± 1.3	14.1 ± 1.3	10	20.5
SHT	450 ± 33	18.6 ± 1.2	16.1 ± 0.7	27	20.5
SHTDS	399 ± 39	17.5 ± 0.5	15.6 ± 0.8	22	20.2

[a] UL94V testing.

which determined the stiffness of these compounds. The addition of 2 wt % EMAA to the HDPE matrix resulted in an increase in the tensile strength of both PEHT and PESHTDS (Fig. 10). This increase could be attributed to the adhesive character of EMMA, which improved the interaction between the HT particles and the polymeric matrix. Moreover, the higher exfoliation of the HT particles achieved in these nanocomposites also contributed to increasing the particle–matrix interaction.

The values of Young's modulus of the EMAA nanocomposites indicate how both particles (pure HT and organically modified HT) exerted a noticeable effect on the stiffness of this ionomer (Fig. 9). This increase could be due, on the one hand, to the higher stiffness of HT particles and, on the other hand, to the formation of more immobilized ionic aggregates. The tensile strength was also increased by the effect of the HT particles, and this confirmed the strong interactions between the HT sheets and the maleic anhydride groups of the ionomer.

Values of the neck propagation strength were higher for the nanocomposites prepared with both the organophilized HT particles and the ionomer. This increase could be due to the higher mobility restriction of the polymeric chains as a result of the increase in the polymer–particle interaction forces in these nanocomposites.

CONCLUSIONS

Nanocomposites based on HDPE and EMAA matrices and pure and organophilized HT particles were prepared by melt compounding. FTIR and XRD analysis provided experimental evidence of the intercalation of dodecyl sulfate ions into the HT sheets, which increased the interlayer spacing and confirmed the organic modification of the particles.

The organophilized HT particles were exfoliated and intercalated in the pure HDPE matrix. The presence of EMAA as a compatibilizer was necessary to achieve the partial exfoliation of the pure HT in HDPE.

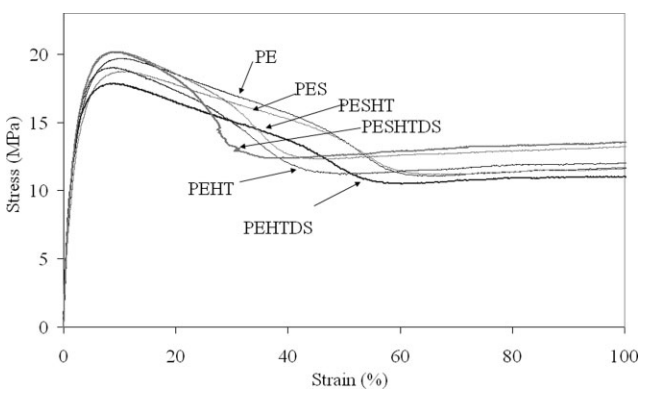

Figure 9 Stress–strain curves of HDPE/HT nanocomposites.

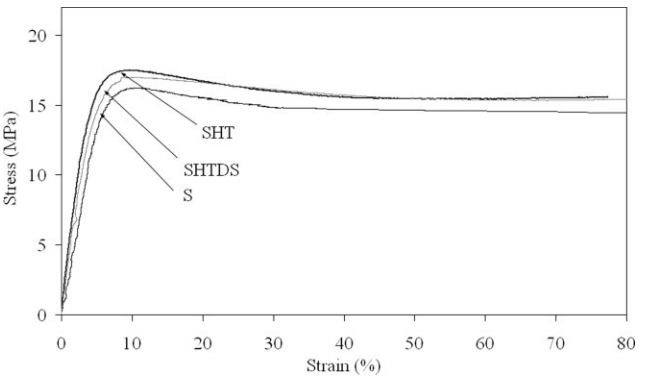

Figure 10 Stress–strain curves of EMAA/HT nanocomposites.

HT particles caused a significant decrease in the MFI values of both HDPE and EMAA.

The resulting HDPE and EMAA nanocomposites exhibited superior thermal properties, and the onset-of-decomposition temperatures of both these polymers increased in air. Even though the LOI values were not improved by the effect of the HT particles, the delay in the dripping time was significant. These results revealed the potential of HT particles as flame-retardant fillers combined with conventional ones.

Because of the formation of more stable ionic aggregates between HT sheets and MAA groups in the EMAA matrix, the resulting nanocomposites exhibited superior mechanical properties, with increased maximum tensile strength, neck propagation strength, and Young's modulus.

References

1. Leroux, F.; Besse, J. P. Chem Mater 2001, 13, 3507.
2. Hsueh, H. B.; Chen, C. Y. Polymer 2003, 44, 5275.
3. Chen, W.; Feng, L.; Qu, B. Solid State Commun 2004, 130, 259.
4. Costa, F. R.; Abdel-Goad, M.; Wagenkmecht, U.; Heinrich, G. Polymer 2005, 46, 4447.
5. He, F. A.; Zhang, L. M. Compos Sci Technol 2007, 67, 3226.
6. Roy, A.; Forano, C.; Besse, J. P. In Layered Double Hydroxides. Present and Future; Rives, V., Ed.; Nova Science: New York, 2001; Chap. 1.
7. Newman, S. P.; Jones, W. New J Chem 1998, 22, 105.
8. Gopakumar, T. G.; Lee, J. A.; Kontopoulou, M.; Parent, J. S. Polymer 2002, 43, 5483.
9. Liang, G.; Xu, J.; Bao, S.; Xu, W. J Appl Polym Sci 2004, 91, 3974.
10. Chen, W.; Qu, B. Chem Mater 2003, 15, 3208.
11. Costa, F. R., Wagenknecht, U.; Jehnichen, D.; Abdel-Goad, M.; Heinrich, G. Polymer 2006, 47, 1649.
12. Sánchez-Valdés, S.; López-Quintanilla, M. L.; Ramírez-Vargas, E.; Medellín-Rodríguez, F. J.; Gutiérrez-Rodríguez, J. M. Macromol Mater Eng 2006, 291, 128.

13. Shah, R. K.; Kim, D. H.; Paul, D. R. Polymer 2007, 48, 1047.
14. Shah, R. K.; Krishnaswamy, R. K.; Takahashi, S.; Paul, D. R. Polymer 2006, 47, 6187.
15. Costa, F. R.; Satapathy, B. K.; Wagenknecht, U.; Weidisch, R.; Heinrich, G. Eur Polym J 2006, 42, 2140.
16. Costache, M. C.; Heidecker, M. J.; Manias, E.; Camino, G.; Frache, A.; Beyer, G.; Gupta, R. K.; Wilkie, C. A. Polymer 2007, 48, 6532.
17. Qiu, L.; Chen, W.; Qu, B. Polymer 2006, 47, 922.
18. Wunderlich, B. New York: Academic, 1990.
19. Vanhoorne, P.; Register, R. A. Macromolecules 1996, 29, 598.
20. Tadano, K.; Hirasawa, E.; Yamamoto, J.; Yano, S. Macromolecules 1989, 22, 226.
21. Kutsumizu, S.; Tadano, K.; Matsuda, Y.; Goto, M.; Tachino, H.; Hara, H.; Hirasawa, E.; Tagawa, H.; Muroga, Y.; Yano, S. Macromolecules 2000, 33, 9044.
22. Costa, F. R.; Wagenknecht, U.; Heinrich, G. Polym Degrad Stab 2007, 92, 1813.